Hierarchy of Fractional Chern Insulators and Competing Compressible States

A. M. Läuchli,[1,2] Zhao Liu,[3,4] E. J. Bergholtz,[5,2] and R. Moessner[2]

[1]*Institut für Theoretische Physik, Universität Innsbruck, A-6020 Innsbruck, Austria*
[2]*Max-Planck-Institut für Physik komplexer Systeme, Nöthnitzer Straße 38, D-01187 Dresden, Germany*
[3]*Beijing Computational Science Research Center, Beijing 100084, China*
[4]*Institute of Physics, Chinese Academy of Sciences, Beijing 100190, China*
[5]*Dahlem Center for Complex Quantum Systems and Institut für Theoretische Physik, Freie Universität Berlin, Arnimallee 14, 14195 Berlin, Germany*

(Received 27 July 2012; revised manuscript received 6 July 2013; published 17 September 2013)

We study the phase diagram of interacting electrons in a dispersionless Chern band as a function of their filling. We find hierarchy multiplets of incompressible states at fillings $\nu = 1/3, 2/5, 3/7, 4/9, 5/9, 4/7, 3/5$ as well as $\nu = 1/5, 2/7$. These are accounted for by an analogy to Haldane pseudopotentials extracted from an analysis of the two-particle problem. Important distinctions to standard fractional quantum Hall physics are striking: in the absence of particle-hole symmetry in a single band, an interaction-induced single-hole dispersion appears, which perturbs and eventually destabilizes incompressible states as ν increases. For this reason, the nature of the state at $\nu = 2/3$ is hard to pin down, while $\nu = 5/7, 4/5$ do not seem to be incompressible in our system.

DOI: 10.1103/PhysRevLett.111.126802 PACS numbers: 73.43.Nq, 71.10.Fd

Introduction.—Following recent proposals of the existence of novel lattice generalizations of fractional quantum Hall (FQH) states, termed fractional Chern insulators (FCI), in (approximately) flat bands exhibiting nonzero Chern numbers [1–3], there has been intense research activity in understanding this phenomenon [4–26].

From the original observation of a FCI state at Chern band filling $\nu = 1/3$ [3–5] (at which the original FQH state was also first observed), a number of questions immediately arises. First, under what conditions can FCIs be observed? Second, what are the states which compete with the FCI states? Third, what are the differences between FCI physics in Chern bands compared to the familiar setting of Landau levels in the continuum appropriate for describing the FQH state in conventional semiconductor heterojunctions, e.g., arising due to the nonuniform Berry curvature in reciprocal space?

This Letter aims to contribute to all of these questions. We start by demonstrating that a nearest-neighbor interaction leads to a FCI state also at $\nu = 2/5$ and $\nu = 1/5$, although the latter fraction has a FCI phase that is substantially less robust than the $\nu = 1/3$ FCI. We account for this with a heuristic derived from considering the two-particle problem in the lattice model. Further, we find evidence of several additional FCI states akin to the hierarchy FQH states familiar from conventional QH physics and its composite fermion [27] hierarchy [28,29] picture.

Turning to the qualitative distinctions from conventional QH physics, we find that in the absence of particle-hole symmetry in a single band, an effective crystal-momentum-dependent potential appears, which shows up in the properties of the single-hole dispersion, and leads to a modulation of the occupation numbers $n(\mathbf{k})$ in the many-body ground state which presage the breakdown of the QH effect. This is reflected by a strong distinction between the many-body states at $\nu = 1/3$ and $\nu = 2/3$ even in the spin-polarized setting that we study.

Our studies use extensive large-scale exact diagonalizations of the many-body Hamiltonian of the lattice systems coupled with analytical considerations. On a more technical level, we address questions of the interplay of topological order and the concomitant finite-size lattice quasi-ground-state degeneracies, as well as the finite-size scaling of the gaps.

Setup.—In order to be specific, we focus on the two-band checkerboard lattice model introduced in Refs. [2,3] and sketched in Fig. 1(a). Here, $t_1 e^{\pm i\phi}$ is a nearest-neighbor hopping with an orientation-dependent complex phase, and t_2 denotes the next-nearest-neighbor hopping

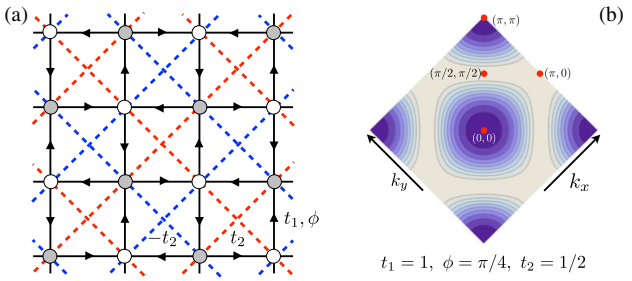

FIG. 1 (color online). (a) Illustration of the checkerboard lattice model with the relevant hopping amplitudes [2,3]. The interaction term is a nearest-neighbor density-density interaction (interaction between pairs of white and grey sites). (b) Berry curvature in the first Brillouin zone for the indicated set of parameters. Dark (light) intensity denotes small (large) Berry curvature.

amplitude. After Fourier transform, the single-electron (kinetic) Hamiltonian reads

$$\mathcal{H} = \sum_{\mathbf{k}\in \mathrm{BZ}} (c^\dagger_{\mathbf{k}A}, c^\dagger_{\mathbf{k}B}) h(\mathbf{k}) (c_{\mathbf{k}A}, c_{\mathbf{k}B})^T, \quad (1)$$

where $h(\mathbf{k})$ is given in Ref. [30]. In the following, we consider the case of $t_1 = 1$, $\phi = \pi/4$, and varying t_2. For $t_2 \neq 0, \infty$, one obtains two separated bands with Chern number ± 1. The Berry curvature in each band can be expressed in terms of the single-particle state in the band $|n^\pm_{\mathbf{k}}\rangle$ via the Berry connection $A^\pm_j(\mathbf{k}) = -i\langle n^\pm_{\mathbf{k}}|\partial_{k_j}|n^\pm_{\mathbf{k}}\rangle$ as $F^\pm_{ij} = \partial_{k_i} A^\pm_j(\mathbf{k}) - \partial_{k_j} A^\pm_i(\mathbf{k})$. The two bands have topologically quantized Chern numbers $C = (1/2\pi)\int_{\mathrm{BZ}} F^\pm_{12}(\mathbf{k}) d^2\mathbf{k} = \pm 1$, while the Berry curvature varies in the Brillouin zone and depends on the microscopic parameters (t_2 in the present case). In Fig. 1(b), we display the Berry curvature for the specific value of $t_2 = 0.5$ [note that the Berry curvature vanishes at (0, 0) and (π, π)].

Interactions.—We consider nearest-neighbor repulsion $H_{\mathrm{int}} = V\sum_{\langle i,j\rangle} n_i n_j$ [cf. caption of Fig. 1(a)] throughout this Letter. If the energy gap between the two bands is large compared to the interaction strength, it is possible to project the interactions into the partially filled band, leading to a projected Hamiltonian of the form

$$H = \sum_{\mathbf{k}_1\mathbf{k}_2\mathbf{k}_3\mathbf{k}_4} V_{\mathbf{k}_1\mathbf{k}_2\mathbf{k}_3\mathbf{k}_4} c^\dagger_{\mathbf{k}_1} c^\dagger_{\mathbf{k}_2} c_{\mathbf{k}_3} c_{\mathbf{k}_4} \quad (2)$$

for two-body interactions. Here, $c_{\mathbf{Q}}$ annihilates an electron with wave function $\phi_{\mathbf{Q}}(\mathbf{r})$ of the single-particle state of the partially filled band with crystal momentum $\mathbf{Q}$. In the following, we take the flat band limit, i.e., drop the residual energy dispersion in the band, as we wish to highlight the new phenomena arising due to the nonconstant Berry curvature, as opposed to remnant energy dispersion.

Particle-hole asymmetry and two-particle analysis.—It is enlightening to consider the two simplest interacting cases, namely, the single-hole and the two-particle problems. Performing a particle-hole transformation $c_{\mathbf{k}} \to c^\dagger_{\mathbf{k}}$ within one of the bands, the projected Hamiltonian (2) transforms to

$$H \to \sum_{\mathbf{k}_1\mathbf{k}_2\mathbf{k}_3\mathbf{k}_4} V^*_{\mathbf{k}_1\mathbf{k}_2\mathbf{k}_3\mathbf{k}_4} c^\dagger_{\mathbf{k}_1} c^\dagger_{\mathbf{k}_2} c_{\mathbf{k}_3} c_{\mathbf{k}_4} + \sum_{\mathbf{k}} E_h(\mathbf{k}) c^\dagger_{\mathbf{k}} c_{\mathbf{k}}, \quad (3)$$

which includes an effective single-hole energy $E_h(\mathbf{k}) = 4\sum_{\mathbf{m}} V_{\mathbf{mkmk}}$ (adopting a convention under which $V_{\mathbf{klmn}}$ is antisymmetric under exchange of its indices). This term amounts to a trivial overall energy shift in a Landau level. By contrast, it introduces an effective dispersion even for an entirely flat Chern band. We display $E_h(\mathbf{k})$ in Fig. 2(a) for $t_2 = 0.5$. As we will demonstrate below, this particle-hole asymmetry generally leads to a deformation of $n(\mathbf{k})$ and in fact dominates the physics near $\nu = 1$, i.e., in the dilute-hole limit. Note that for our checkerboard example, the energy spectrum is particle-hole invariant under $\nu \leftrightarrow 2 - \nu$.

Next, we consider the two-particle problem: In Fig. 2(b), we display the nonzero eigenvalues of the two-particle problem along a path in the Brillouin zone for the nearest-neighbor interaction for $t_2 = 0.5$. The spectrum depends on the total momentum $\mathbf{K} = \mathbf{k}_1 + \mathbf{k}_2$ underscoring the lack of translation invariance in reciprocal space. We observe two dominant eigenvalues of mean value $\approx 0.4\ V$ which remain nonzero throughout the Brillouin zone, while there is also a second set of two eigenvalues about 10 times smaller which vanish as $\mathbf{K} \to (0,0)$. All other eigenvalues are strictly zero [31]. Considering the analogous two-particle problem in the continuum, one finds that the eigenvalues are independent of the center of mass momentum $\mathbf{K}$ and that one can identify these eigenvalues with Haldane's pseudopotenial parameters $\mathcal{V}_m$ (m odd for fermions), well known in Landau levels [28]. The multiplicity of these energy levels [31] motivates a suggestive pseudopotential analogy in which we label the two nonzero pairs of eigenvalues of the projected two-particle Chern band problem as "pseudopotentials" $\mathcal{V}_1$ (the larger pair) and $\mathcal{V}_3$ (the smaller pair), as indicated in Fig. 2(b).

Hierarchy states and the phase diagram.—To investigate the full interacting many-body problem, we have performed extensive exact diagonalization studies on a large number of finite samples with rectangular shapes (as in previous numerical studies of FCI) as well as tilted samples, where the spanning vectors of the samples need not be aligned with the lattice axes. The latter choice of samples allows us to study a considerably larger number of clusters with aspect ratio close to one. The list of considered clusters can be found in the Supplemental Material [31].

The pseudopotential analogy introduced above suggests a hierarchy of incompressible states at $\nu = p/q \geq 1/3$, q odd, due to the relatively large energy scale $\mathcal{V}_1$. In

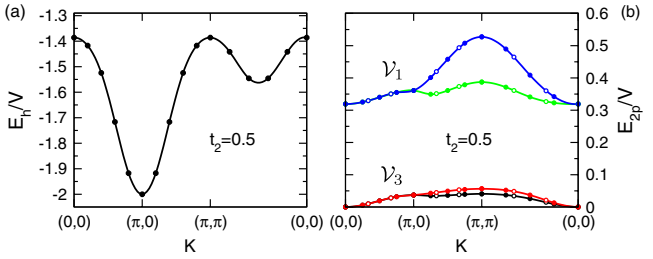

FIG. 2 (color online). (a) Energy of a single hole in the fully filled lower band $E_h(\mathbf{K}) := E(N_p = N_s - 1, \mathbf{K}) - E(N_p = N_s, \mathbf{0})$. (b) Nonzero eigenvalues $E(N_p = 2, \mathbf{K})$ of the two-particle problem on a representative path through the Brillouin zone for $t_2 = 0.5$. In general, there are four nonzero energies except at $\mathbf{K} = (0, 0)$, where there are only two finite energies. Circles are data for (b) 6×6 (empty circles) and 8×8 (filled circles) unit cells [(a) 10×10 unit cells], and the lines are guides to the eye.

particular, we have looked for the $m = 1$ composite fermion branch at $\nu = p/(2mp + 1)$ [27] with rather clear evidence of FCI states at $\nu = 2/5, 3/7, 4/9$ as well as their $1 - \nu$ relatives at $\nu = 5/9, 4/7, 3/5$, beyond the $\nu = 1/3$ state already discussed in the literature [3–5]. Data of the low-energy spectrum of at least two samples for each fraction are displayed in the Supplemental Material [31]. Here, we provide strong evidence for a stable incompressible $\nu = 2/5$ state, as shown in Figs. 3(a)–3(c). In Fig. 3(a), we present the spectral flow of the five ground-state manifold levels upon flux insertion for two different samples. The ground-state manifold (filled symbols) does not mix with excited states (empty symbols) and returns to the initial spectrum upon insertion of five flux quanta. This provides strong evidence for a state with quantized Hall conductance. In Fig. 3(b), we display the finite-size scaling of the energy spread of the five states in the ground-state manifold for different samples. We plot the energy splitting as a function of the inverse topological extent $1/W$ (as defined in the Supplemental Material [31]; in short, it counts the number of straight discrete $\mathbf{\Delta k}$ steps one has to follow in momentum space to return to the origin), which can become quite small (as small as $1/25$) for our tilted samples. Note that the topological extent is not in general equivalent to the geometrical extent. In particular, the samples with $W = 10, 20, 25$ have a geometrical aspect ratio equal to one. We also stress that the five ground states are systematically found in the sectors predicted by the counting rule developed in Refs. [5,9] and which we generalized for tilted samples [31]. In the case of tilted samples, the ground-state sectors show a great variability, depending on the cluster geometry, which is an argument against the formation of a charge density wave state, which should exhibit a unique set of degenerate momenta dictated by the spatial symmetry breaking of the charge density wave. Finally, in Fig. 3(c), we show the finite-size scaling of the gap from the ground state to the first excited state as a function of inverse system size $1/N_s$. Our data show non-negligible finite-size effects but convincingly point towards a finite excitation gap of the order of $V/30$ in the thermodynamic limit. This is in contrast to recent claims of a vanishing gap based on smaller system sizes [17,20].

Next, we turn to fractions below $\nu = 1/3$. According to the pseudopotential analogy, our nearest-neighbor interactions generate a finite $\mathcal{V}_3$, albeit roughly a factor of 10 smaller than $\mathcal{V}_1$. We would thus expect to find a stable $\nu = 1/5$ state with associated energy scales significantly smaller than those of the $\nu = 1/3$ state. Indeed, we find strong evidence for a $\nu = 1/5$ FCI state, as shown in Figs. 3(d)–3(f). In particular, the finite-size effects of the ground-state manifold splitting shown in Fig. 3(e) behave qualitatively similarly to the $\nu = 2/5$ case in Fig. 3(b), and the energy gap to excited states extrapolates to a value of the order of $V/200$. We furthermore find some mild evidence for a $\nu = 2/7$ state [31], which is stabilized by $\mathcal{V}_3$.

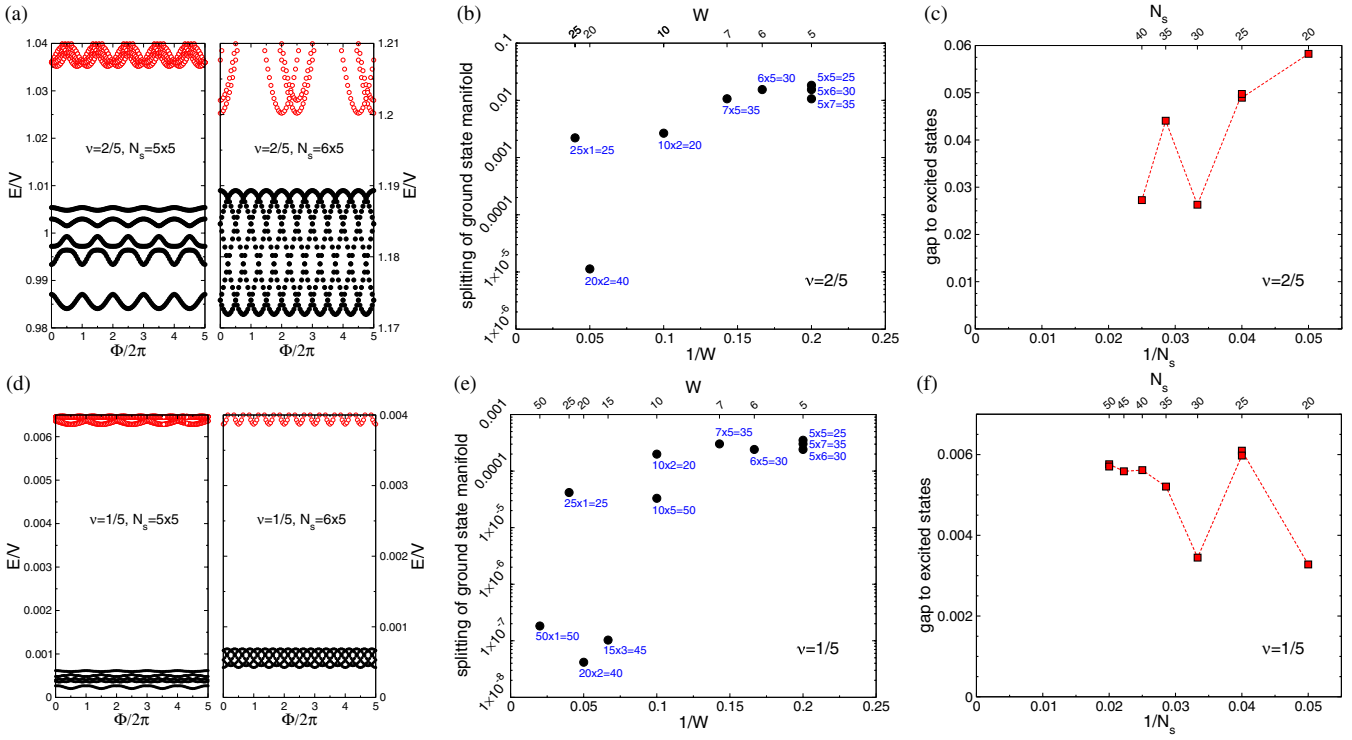

FIG. 3 (color online). (a)–(c) Numerical evidence for a fractional Chern insulator state at $\nu = 2/5$. (d)–(f) Numerical evidence for a fractional Chern insulator state at $\nu = 1/5$. For details, see the main text. Here, we focus on $t_2 = 0.5$, which is close to the value where the variance of the Berry curvature is minimal. See Table I for the samples that we consider in (c) and (f).

Effect of the single-hole energy.—When numerically exploring the phase diagram, we discovered that several particle-hole conjugate states of stable low-density FCI fractions do not seem to be realized; for example, we find it difficult to systematically observe the required ground-state degeneracy for $\nu = 2/3$, while for $\nu = 5/7$ and $\nu = 4/5$, the required degeneracy is absent. An enlightening way to understand this finding is to monitor the filling dependence of the momentum space occupation number $n(\mathbf{k}) = \langle c^\dagger_{\mathbf{k}} c_{\mathbf{k}} \rangle$ when plotted as a function of the single-hole energy $E_h(\mathbf{k})$ introduced before (see Fig. 4), where the occupancy $n(\mathbf{k})$ in the incompressible many-body state clearly tracks $E_h(\mathbf{k})$. Note that we display $n(\mathbf{k})$ for all momenta in the Brillouin zone but plot the value $n(\mathbf{k})$ at the position $E_h(\mathbf{k})$ on the x axis. The data collapse onto a single curve, which is roughly linear for the incompressible fractions, is quite remarkable. The role of the interaction-induced effective single-particle dispersion is thus to significantly distort the momentum space occupancy as the filling increases. When the distortion becomes too strong, the incompressible FCI state becomes unstable and a compressible state with a Fermi-like $n(\mathbf{k})$ distribution takes over. We expect these compressible Fermi-liquid-like states to show a large, but nonquantized, anomalous Hall effect.

It is instructive to compare our results with what is known from conventional FQH physics. For intermediate filling fractions in the lowest Landau level, both experiment [32] and theory [33] suggest that the stability of the FQH states towards disorder, temperature, etc., is essentially determined by the denominator q of the filling fraction (for odd q), implying a self-similar structure in the clean zero-temperature limit. Corrections to the self-similar structure in "real" systems are minor and include effects due to an instability towards Wigner crystallization at low filling fractions and particle-hole symmetry breaking effects. (Landau level mixing, etc.) The main features are qualitatively similar to what we find in the lattice system. However, in the Chern insulator case, the corrections are more substantial. In particular, there is nothing like a "clean" limit, as the Berry curvature effects necessarily destroy weak states, and the compressible competing states discussed above prevail. Moreover, due to the explicit particle-hole asymmetry within the band, we find that FCI states are absent for $\nu \gtrsim 2/3$.

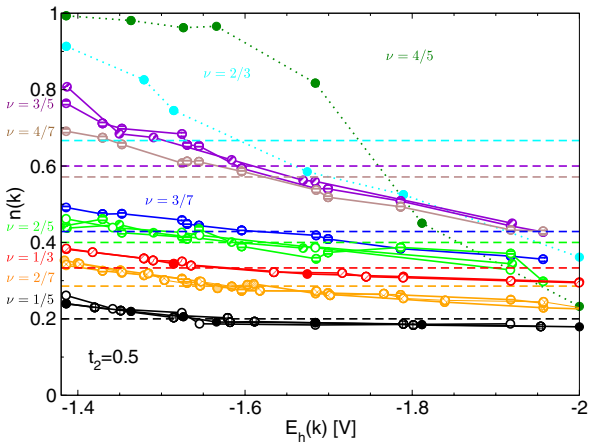

FIG. 4 (color online). Momentum space orbital occupation $n(\mathbf{k}) = \langle c^\dagger_{\mathbf{k}} c_{\mathbf{k}} \rangle$ plotted as a function of the single-hole energy $E_h(\mathbf{k})$. Different colors denote different fractions, while the symbols at the same fraction label different clusters. The dashed horizontal lines serve as reference values for a constant $n(\mathbf{k})$ at the same filling fraction. As the filling ν is increased, $n(\mathbf{k})$ displays a more pronounced (roughly linear) correlation with $E_h(\mathbf{k})$. Dotted lines ($\nu = 2/3$, $\nu = 4/5$) denote fractions which are most likely compressible, non-FCI states.

Discussion.—The question of to what extent fractional Chern insulators are "nothing but" FQH states on the lattice is fundamental to this rapidly developing field: it combines the questions of where to find a FCI with how to diagnose it and how to theoretically describe it, before being able to address differences to the "weak-field" continuum Landau level physics.

The FCI states we thus found, as well as their respective stabilities, are naturally organized with the aid of the hierarchy concept developed for the FQH. To obtain this information, we have developed new diagnostics, including an adaptation of Haldane's pseudopotentials, strongly suggesting a common field-theoretic description for the two phenomena. At the same time, a particularly noteworthy *negative* result is our observation, at odds with some previous treatments, that FCIs do not generically come with a constant occupation number of the flat band orbitals in reciprocal space.

Indeed, this phenomenon arises even for perfectly flat (dispersionless) bands, as a result of a nonuniform Berry curvature, which appears as a potent driving force for the destruction of FCI states by acting as a $\mathbf{k}$-dependent chemical potential of a strength tuned by the electron density of the flat band, removing particle-hole symmetry in a lattice-specific manner. Our study provides a first glimpse of the competing states.

Clearly, much further work on each of these points is warranted, especially in the light of promising experimental prospects to observe such states in optical lattices with artificial magnetic fields [21,34–36].

We acknowledge useful discussions with Masud Haque. E. J. B. was supported by the Alexander von Humboldt Foundation and by the Emmy Noether Program (BE 5233/1-1) of the German Research Foundation (DFG). Z. L. is supported by the China Postdoctoral Science Foundation Grant No. 2012M520149. Simulations have been performed on machines of the platform "Scientific computing" at the University of Innsbruck—supported by the BMWF—and on the PKS-AIMS and vip cluster at the MPG RZ Garching.

Note added.—Recently, we became aware of three papers which also provide evidence for FCI states beyond the Laughlin states [16,17,20].

[1] E. Tang, J.-W. Mei, and X.-G. Wen, Phys. Rev. Lett. **106**, 236802 (2011).

[2] K. Sun, Z. Gu, H. Katsura, and S. Das Sarma, Phys. Rev. Lett. **106**, 236803 (2011).

[3] T. Neupert, L. Santos, C. Chamon, and C. Mudry, Phys. Rev. Lett. **106**, 236804 (2011).

[4] D. N. Sheng, Z. Gu, K. Sun, and L. Sheng, Nat. Commun. **2**, 389 (2011).

[5] N. Regnault and B. A. Bernevig, Phys. Rev. X **1**, 021014 (2011).

[6] Y.-F. Wang, Z.-C. Gu, C.-D. Gong, and D. N. Sheng, Phys. Rev. Lett. **107**, 146803 (2011).

[7] X.-L. Qi, Phys. Rev. Lett. **107**, 126803 (2011).

[8] S. A. Parameswaran, R. Roy, and S. L. Sondhi, Phys. Rev. B **85**, 241308(R) (2012); M. O. Goerbig, Eur. Phys. J. B **85**, 15 (2012).

[9] B. A. Bernevig and N. Regnault, Phys. Rev. B **85**, 075128 (2012).

[10] Y.-F. Wang, H. Yao, Z.-C. Gu, C.-D. Gong, and D. N. Sheng, Phys. Rev. Lett. **108**, 126805 (2012).

[11] Y.-L. Wu, B. A. Bernevig, and N. Regnault, Phys. Rev. B **85**, 075116 (2012).

[12] G. Murthy and R. Shankar, arXiv:1108.5501; Phys. Rev. B **86**, 195146 (2012).

[13] J. McGreevy, B. Swingle, and K.-A. Tran, Phys. Rev. B **85**, 125105 (2012); A. Vaezi, arXiv:1105.0406.

[14] For related models and suggested realizations, see, e.g., J. W. F. Venderbos, M. Daghofer, and J. van den Brink, Phys. Rev. Lett. **107**, 116401 (2011); X. Hu, M. Kargarian, and G. A. Fiete, Phys. Rev. B **84**, 155116 (2011); F. Wang and Y. Ran, Phys. Rev. B **84**, 241103(R) (2011); P. Ghaemi, J. Cayssol, D. N. Sheng, and A. Vishwanath, Phys. Rev. Lett. **108**, 266801 (2012); M. Trescher and E. J. Bergholtz, Phys. Rev. B **86**, 241111(R) (2012); S. Yang, Z.-C. Gu, K. Sun, and S. Das Sarma, Phys. Rev. B **86**, 241112(R) (2012).

[15] Y.-L. Wu, N. Regnault, and B. A. Bernevig, Phys. Rev. B **86**, 085129 (2012).

[16] J. W. F. Venderbos, S. Kourtis, J. van den Brink, and M. Daghofer, Phys. Rev. Lett. **108**, 126405 (2012).

[17] T. Liu, C. Repellin, B. A. Bernevig, and N. Regnault, Phys. Rev. B **87**, 205136 (2013).

[18] B. A. Bernevig and N. Regnault, arXiv:1204.5682.

[19] T. Scaffidi and G. Möller, Phys. Rev. Lett. **109**, 246805 (2012).

[20] Y.-H. Wu, J. K. Jain, and K. Sun, Phys. Rev. B **86**, 165129 (2012).

[21] N. Y. Yao, C. R. Laumann, A. V. Gorshkov, S. D. Bennett, E. Demler, P. Zoller, and M. D. Lukin, Phys. Rev. Lett. **109**, 266804 (2012).

[22] A. G. Grushin, T. Neupert, C. Chamon, and C. Mudry, Phys. Rev. B **86**, 205125 (2012).

[23] Y.-F. Wang, H. Yao, C.-D. Gong, and D. N. Sheng, Phys. Rev. B **86**, 201101(R) (2012).

[24] Z. Liu, E. J. Bergholtz, H. Fan, and A. M. Läuchli, Phys. Rev. Lett. **109**, 186805 (2012).

[25] M. Barkeshli and X.-L. Qi, Phys. Rev. X **2**, 031013 (2012).

[26] D. Xiao, W. Zhu, Y. Ran, N. Nagaosa, and S. Okamoto, Nat. Commun. **2**, 596 (2011).

[27] J. K. Jain, Phys. Rev. Lett. **63**, 199 (1989); J. K. Jain, *Composite Fermions* (Cambridge University Press, Cambridge, England, 2007).

[28] F. D. M. Haldane, Phys. Rev. Lett. **51**, 605 (1983).

[29] B. I. Halperin, Phys. Rev. Lett. **52**, 1583 (1984).

[30] $h(\mathbf{k}) = \sum_i d_i(\mathbf{k})\sigma_i$, with $d_x(\mathbf{k}) = 4t_1 \cos(\phi)\cos(k_x/2) \times \cos(k_y/2)$, $d_y(\mathbf{k}) = 4t_1 \sin(\phi)\sin(k_x/2)\sin(k_y/2)$, and $d_z(\mathbf{k}) = 2t_2[\cos(k_x) - \cos(k_y)]$, and σ_i are the Pauli matrices.

[31] See Supplemental Material at http://link.aps.org/supplemental/10.1103/PhysRevLett.111.126802 for details.

[32] See, e.g., W. Pan, H. L. Stormer, D. C. Tsui, L. N. Pfeiffer, K. W. Baldwin, and K. W. West, Phys. Rev. Lett. **90**, 016801 (2003).

[33] E. J. Bergholtz, T. H. Hansson, M. Hermanns, and A. Karlhede, Phys. Rev. Lett. **99**, 256803 (2007).

[34] M.-C. Chang and Q. Niu, Phys. Rev. B **53**, 7010 (1996).

[35] M. Aidelsburger, M. Atala, S. Nascimbène, S. Trotzky, Y.-A. Chen, and I. Bloch, Phys. Rev. Lett. **107**, 255301 (2011).

[36] H. M. Price and N. R. Cooper, Phys. Rev. A **85**, 033620 (2012).